Recent Advances in Slow Heavy Particle Induced Electron Emission

HP. Winter[1,⋆], F. Aumayr[1], H. Winter[2] and S. Lederer[1]

[1]Institut für Allgemeine Physik, TU Wien, A-1040, Austria
[2]Institut für Physik, Humboldt-Universität zu Berlin, Germany

Abstract

We present recent developments for electron emission induced by impact of slow (projectile velocity $\leq$ 1 a.u. = 2.18×10^6 m/s) atoms, molecules, and singly and multiply charged ions on atomically clean monocrystalline metal and insulator surfaces. We show, in particular, that with grazing incident projectiles on monocrystalline flat surfaces the coincident measurement of projectile energy loss with the number of emitted electrons, the electron yields caused by potential and kinetic emission can be distinguished. Furthermore, for grazing impact of neutral ground state atoms on monocrystalline flat metal surfaces a very precise determination of the small total electron yield near the kinetic emission threshold can be achieved, and the measured yields are in good agreement with a classical model for electron emission from binary collisions of projectiles with quasi-free metal electrons above the target surface. We also present some results on slow molecular projectile non-proportionality effects in kinetic emission. Finally, we mention as two novel applications of KE a surface structure determination based on KE by grazing-incident ions or atoms, and a method for evaluation of mixed ion beam fractions for different ion species with nearly equal charge-to-mass ratios.

Contents

⋆ E-mail: winter@iap.tuwien.ac.at

1. General Aspects of Kinetic Emission (KE) and Potential Emission (PE) – Scope of the Present Report

Processes induced by impact of slow heavy particles on solid surfaces (neutral/ionized atoms or molecules; impact velocity typically far below 1 a.u. = 25 keV/amu = 2.18×10^6 m/s) are highly relevant for plasma- and surface physics and -technology (Hasselkamp, 1992). Nature and intensity of these processes depend both on the kinetic and the potential (i.e. internal) energy carried by the projectile toward the surface.

1.1. Kinetic Electron Emission (KE)

In most practical applications the kinetic energy of a projectile is of higher relevance than the potential energy, as, e.g., for kinetic emission (KE) (Hasselkamp, 1992; Schou, 1988; Rösler and Brauer, 1991; Baragiola, 1993), ion-surface scattering and kinetic sputtering (Sigmund, 1993; Gnaser, 1999). For inducing KE, the projectile needs a minimum velocity or kinetic energy (KE

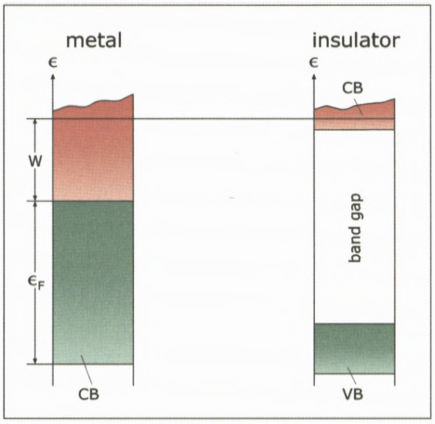

Figure 1. Energy levels for quasi-free electron metal (left) and wide-band gap insulator (right). CB: conduction band (with empty region in red), VB: valence band. Horizontal line: vacuum level, EF: Fermi energy, W: surface work function.

threshold) which depends on the projectile and target species. In general, this KE threshold cannot be clearly identified. Precise determination of the electron yield which disappears at the KE threshold is not a simple task, because common techniques for electron yield measurement involve the electrical currents of impinging projectiles and ejected electrons. The absolute measurement of neutral projectile fluxes requires rather specific methods. Different processes can contribute to KE and their relative importance depends strongly on the given situation.

For normal incidence on metal targets, both the momentum transfer from projectiles onto quasi-free metal electrons and electron promotion into the continuum in close collisions with target atom cores may excite electrons inside the target bulk. In insulator targets there are no quasi-free electrons and KE can then only arise from close projectile-target particle collisions. Figure 1 compares the principally different surface-densities-of-states of a quasi-free electron metal and a wide-band gap insulator surface.

In the present review we deal with recent studies for grazing incidence of neutral atoms and singly and multiply charged atomic ions on exclusively atomically clean metal and insulator surfaces. We discuss related total electron yields derived from measured electron number statistics (ES), without considering energy and angular distributions of the emitted electrons. The considered projectile impact energy is restricted to a few keV/amu (for electron emission induced by faster ions we refer to the review of H. Rothart in this book).

Sections 2 and 3 deal with KE and PE studies for monocrystalline Au(111), Al(111) and LiF(001) surfaces where differences in the surface-density-of-states

play a decisive role. In either case, electrons excited inside the solid diffuse toward the surface and only a fraction of them can escape into vacuum. KE involves at least three steps, i.e. electron excitation in the target bulk, transport of some of these electrons to the surface and passage of a fraction of the originally excited electrons over the solid-vacuum barrier (Hasselkamp, 1992; Rösler and Brauer, 1991). We have restricted ourselves to measurements for PE and KE from *collisions in the surface selvedge* (region at and above the topmost plane of surface atoms). In this case the KE yield depends almost exclusively on the primary excitation mechanism (step 1), and in contrast to the more common near-normal incidence conditions the two other steps for KE are of minor importance.

Grazing incidence conditions permit a fine tuning of the distance of closest projectile approach toward the surface, corresponding to an impact parameter selection in atomic collisions. Combined with the technique of electron emission statistics (ES, see Section 2) this opens the possibility for KE measurements with a so far not achieved sensitivity and accuracy, being of foremost importance for near-KE threshold studies.

In addition to their kinetic energy, singly and multiply charged ions (MCI) Z^{q+} also carry the potential energy which had to be spent for removing the respective number of electron(s) from the initially neutral atom. The same potential energy will be released if the charged projectiles are neutralized upon impact on the surface, giving rise to (additional) potential electron emission (PE) (Baragiola, 1993; Hagstrum, 1954a, 1954b; Arnau et al., 1997; Winter, 2002); see also Figure 2. Apart from producing PE, the potential ion energy causes for some materials desorption of near-surface particles ("potential sputtering") (Neidhart et al., 1995; Sporn et al., 1997; Aumayr and Winter, 2004).

1.2. Potential Electron Emission (PE)

PE results from fast electronic transitions (rates $\geq 10^{14}$ s^{-1}) between surface and empty projectile states, which require no minimum impact velocity and start before the ion has actually touched the surface (Hagstrum, 1954a, 1954b). The PE yield increases strongly with the projectile potential energy, i.e. its charge state q. At higher impact velocity also KE will produce slow electrons which cannot simply be distinguished from the PE contribution. Various one- and two-electron transitions can be relevant for PE.

Resonant neutralization transfers electrons into empty states of the ion which overlap occupied surface valence band states. For MCI impact sequential resonance neutralization generates multiply-excited particles (Arifov et al., 1973) termed "hollow atoms" (Briand et al., 1990).

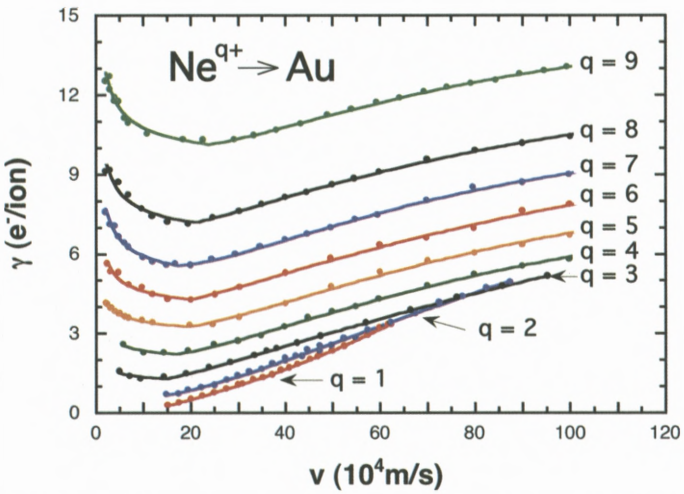

Figure 2. Total electron yields γ *versus* ion velocity v measured for impact of singly and multiply charged Ne ions on atomically clean polycrystalline gold (Eder et al., 1999). Observed electron yields result from KE (yield increases monotonically with impact velocity from the threshold on) and PE (respective yield increases with ion charge state but slightly decreases with impact energy).

Resonant ionization as the inverse process to resonance neutralization transfers electrons from projectile states into empty states with binding energy below the surface work function W.

Auger neutralization (sometimes named *Auger capture*) can give rise to electron ejection from the surface valence band if the available potential energy exceeds twice the surface work function W. One electron is captured by the ion and another one ejected with a kinetic energy defined by the common energy balance. The electron energy distribution corresponds to the self-convolution of the surface-electronic-density-of-states.

Auger de-excitation of projectiles can take place if after resonance or Auger neutralization their excitation energy is still larger than W. Excited projectile electrons interact with target electrons and the latter are ejected and the former demoted, or other target electrons are captured into the projectile and originally excited electron of the projectile ejected. In contrast to Auger neutralization, electron energy distributions resulting from Auger de-excitation are directly correlated with the surface-density-of states.

By incorporating these different electronic transitions into an adiabatic model (no coupling between electronic and nuclear motion), the total slow electron yield can be calculated (Hagstrum, 1954a, 1954b, 1956). Transition rates increase exponentially with decreasing ion-surface distance, according to the overlap between

the surface-density-of-states and the projectile-based electronic wave functions. Consequently, these transitions start most probably from the Fermi edge of the surface-density-of-states. Assuming transition probabilities as independent of the impact velocity, neutralization of singly charged ions occurs most probably at a distance of a few Angstroms. Neutralization of an MCI Z^{q+} can, however, already start at a considerably larger distance which increases with the charge state q (see below). MCI may capture a sizeable number of electrons from the surface within a rather short time (typically about ten fs), which will give rise to *autoionization* of the transiently multiply-excited particles. Here, one or more electrons are ejected into vacuum, while other projectile electrons are demoted into lower lying states. Projectile autoionization was first observed for transiently formed doubly-excited atoms in the surface impact of He^{2+} or metastable He^{+} (Hagstrum and Becker, 1973). Electron energy distributions resulting from autoionization are not related to the target surface-density-of-states.

Quasi-resonant neutralization is a near-resonant transition between target- and projectile core states which can only occur in close collisions by a strong overlap of the inner electronic orbitals. This process may occur in the late stage of MCI neutralization in the bulk.

Radiative de-excitation of excited projectile states formed by resonance of Auger neutralization of singly charged ions is much less probable than Auger de-excitation, since the respective transition rates are orders of magnitude smaller than for Auger transitions. However, the radiative transition rates increase with about the fourth power of the projectile core charge (Bethe and Salpeter, 1957), whereas the Auger transition rates are not strongly affected by electron-core interaction. Therefore, in the final steps of the MCI de-excitation which involve the recombination of inner-shell vacancies, apart from Auger electron emission also soft X-ray emission can become probable (see below).

Based on the above concepts our present understanding of MCI-surface interaction has been sketched in Figure 3. Neutralization of MCI starts by forming transient multiple-excited species which carry empty inner shells and have thus been called a "Hollow Atom". This name was first used (Briand et al., 1990) for explaining the projectile-characteristic soft X-ray emission observed in the surface impact of MCI. The X-rays are produced in the late stage of the hollow-atom decay inside the target bulk, whereas most of the slow electrons will be emitted already before the hollow atom has touched the surface (Arnau et al., 1997). In this way a MCI extracts a number of electrons from the surface and eventually becomes neutral. During this neutralization, slow electrons are emitted via autoionzation. Eventually, the full MCI potential energy will be deposited during a rather short time (typically less than hundred femtoseconds) within a very small

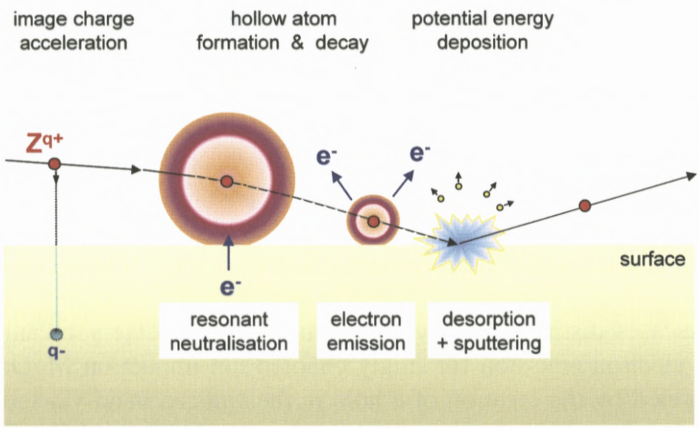

Figure 3. Schematic characterization of neutralization steps for a slow MCI approaching a surface, with formation of a hollow atom, its decay and possible KE (Winter and Aumayr, 2002).

area (typically one nm squared). This neutralization sequence can be explained by the so-called "classical over-the-barrier model" (Burgdörfer et al., 1991). If the hollow atom gets closer to the surface, it will become screened by target electrons which further accelerates its neutralization and de-excitation sequence.

Desorption and potential sputtering (Neidhart et al., 1995; Sporn et al., 1997; Aumayr and Winter, 2004) do only occur for certain insulator materials and gas-covered surfaces.

Once inside the solid, the so far remained inner shell vacancies in the strongly screened hollow atom will now also be filled, which gives rise to emission of projectile-characteristic fast Auger electrons and/or soft X-rays (see above), depending on the respective fluorescence yield. The different projectile recombination- and relaxation processes cannot be easily distinguished from each other, since some of the fast Auger electron emission may already occur before close surface contact and slow electron emission can continue after penetration of the surface. However, the slow electrons carry the information about the hollow-atom development above and at the target surface, whereas the fast Auger electrons and/or soft X-rays are signatures for the final hollow-atom development below the surface (Arnau et al., 1997).

1.3. Combined Kinetic and Potential Electron Emission

If the ion kinetic energy stays well above the KE threshold (Hasselkamp, 1992), total electron yields will result both from PE and KE, and the relative importance of both contributions will be difficult to distinguish except in the following cases.

(a) For projectile ions with a kinetic energy well below the KE threshold (exclusive PE);
(b) if the potential energy greatly exceeds the kinetic energy (dominant PE);
(c) for neutral ground-state projectiles of any velocity (exclusive KE).

In Section 2 we will demonstrate how for the special case of grazing projectile incidence the coincident measurement of electron emission and projectile energy loss permits separation of PE and KE contributions, even if both are of comparable size.

In some cases distinction between KE and PE is not very meaningful. One example is electron emission for singly charged ion impact on MgO, which has been interpreted by the creation of a hole in the valence band via resonant electron capture, followed by Auger neutralization of this hole (PE related effect) (Matulevich and Zeijlmans van Emmichoven, 2004). An alternative explanation involves production of a surface exciton via electron promotion in collisions with O^- target ions (a kinetic effect) followed by autoionization of the exciton (an Auger-type effect) (Riccardi et al., 2004).

Another effect concerns the excitation of plasmons. Sufficiently fast particles (electrons, ions) can excite plasmons in a solid (Raether, 1988). Another plasmon excitation process has recently been observed for slow ion impact on metal surfaces (Baragiola and Dukes, 1996; Stolterfoht et al., 1998).

For this to occur, either the ion potential energy needs to be sufficiently high ("potential excitation of plasmons"), or it proceeds as a secondary process which is caused by fast electrons from KE. Clear signature for plasmon excitation is the subsequent one-electron decay with a characteristic feature in the electron energy distribution (Raether, 1988; Baragiola and Dukes, 1996; Stolterfoht et al., 1998; Eder et al., 2001). Slow-ion induced plasmons can therefore result from the potential and/or the kinetic projectile energy.

2. KE and PE for Grazing Incidence of Slow MCI on Single Crystal Surfaces

2.1. Experimental Aspects

The total electron yield γ (mean number of electrons emitted for single projectile impacts) from KE and/or PE is usually determined from the fluxes of projectiles I_p and emitted electrons $I_e = \gamma \cdot I_p/q$ ("current measurement"; see Hasselkamp, 1992). For charged projectiles this can be simply accomplished by the measurement of target currents for different target bias (with and without electrons leaving

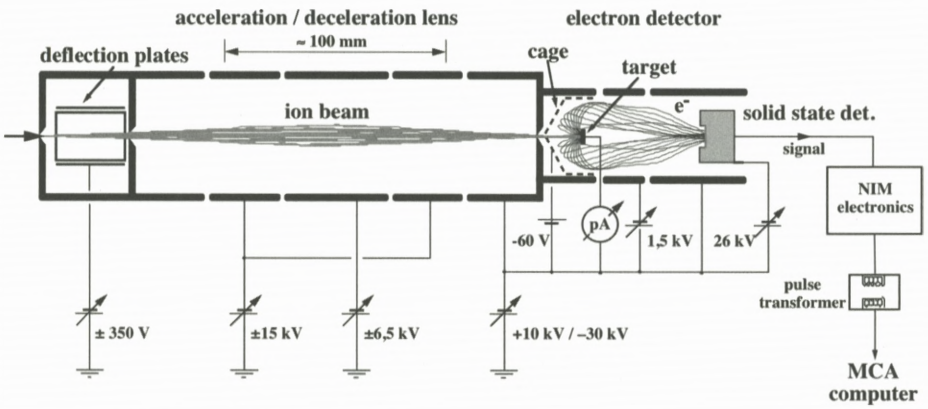

Figure 4. Experimental setup for measuring the electron number statistics (ES) (Eder et al., 1997).

the surface). Here one must avoid possible contributions from charged particle reflection, secondary ion emission and spurious electron production by reflected or scattered projectiles or electrons. Primary ion currents should be at least in the nA range which can become a problem for highly charged ions. Neutral projectile fluxes can either be determined via KE if the respective yield is already known, or by means of sensitive calorimetry with a bolometer.

Another very useful method for total electron yield measurements utilizes the electron number statistics (ES), i.e. the probability distribution W_n for ejection of $1, 2, \ldots, n$ electrons per incident projectile. From this ES the total electron yield γ is simply obtained as the first moment of the W_n distribution, if the probability W_0 for no electron emission is also known (see below; Lakits et al., 1989a; Aumayr et al., 1991; Kurz et al., 1992, 1993; Eder et al., 1997). Figure 4 shows a setup for ES measurements for near-normal particle incidence. Incoming ions are brought to the desired impact energy by a four-cylinder lens before hitting the target surface, but their lowest achievable impact energy is determined by image charge acceleration toward the surface (Aumayr et al., 1993a; Winter et al., 1993). Electrons ejected from the target with an energy below about 50 eV into the full 2π solid angle are back-bent by a highly transparent (96%) conical electrode and accelerated toward a surface barrier detector at 20 kV with respect to the target. The probability W_0 that no electron is emitted cannot be directly measured but becomes practically negligible for $\gamma \geq 3$. However, for small electron yields W_0 is the dominant ES component, and without its knowledge no accurate determination of γ by the ES technique is possible.

In Sections 2.2, 2.3 and 3 below we describe ES measurements in coincidence with grazing scattered projectiles, which permit a straightforward evaluation of

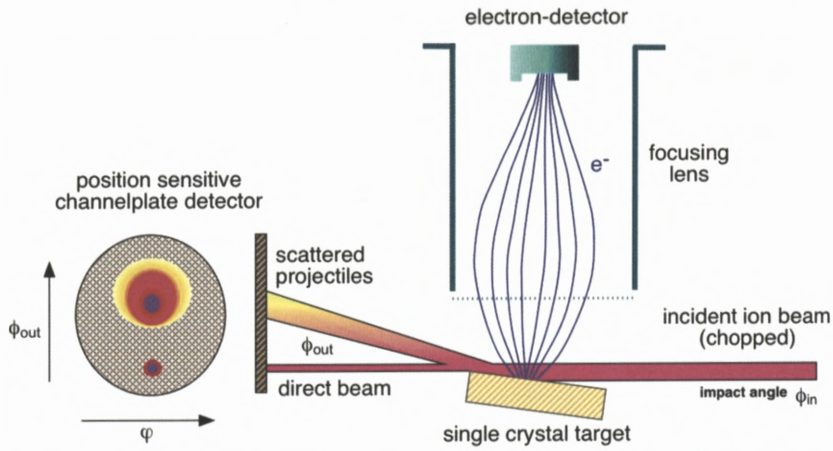

Figure 5. Experimental setup (schematic) for measuring electron number stastistics (ES) in coincidence with scattered projectiles for grazing incidence of slow MCI on a monocrystalline flat target surface (Lemell et al., 1998; Lemell et al., 1999).

W_0 and therewith the precise measurement of very small electron yields. As two other attractive features, the ES technique is also applicable for neutral projectiles and it requires only very small projectile flux (less than 10^4 projectiles/s), which avoids the disturbing charge-up of insulator surfaces (Vana et al., 1995a, 1995b). Apart from its application for measuring γ, the ES are of interest in their own, as they give information on the total number of electrons involved in the particular emission process, and on the related mean single electron emission probability. These two parameters differ significantly for KE and PE processes (Lemell et al., 1995, 1996a; Vana et al., 1995c).

For determination of the relative importance of PE and KE we have performed measurements with slow MCI impinging under a grazing angle of incidence on atomically clean flat monocrystalline target surfaces. In this particular scattering geometry the projectiles interact with the surface along well-defined trajectories (surface channeling; see Winter, 2002). Rather detailed information can be obtained if the electron emission is measured in coincidence with the angular distribution of scattered projectiles (Lemell et al., 1998, 1999), and further insight can be gained if the energy loss of scattered projectiles is also taken into account (Stöckl et al., 2004).

Figure 5 schematically shows a setup by which the energy- and angular distributions of projectiles scattered under grazing incidence from a flat monocrystalline target surface can be observed in coincidence with the ES of ejected electrons. In such a situation neutral scattered projectiles are usually more abundant than

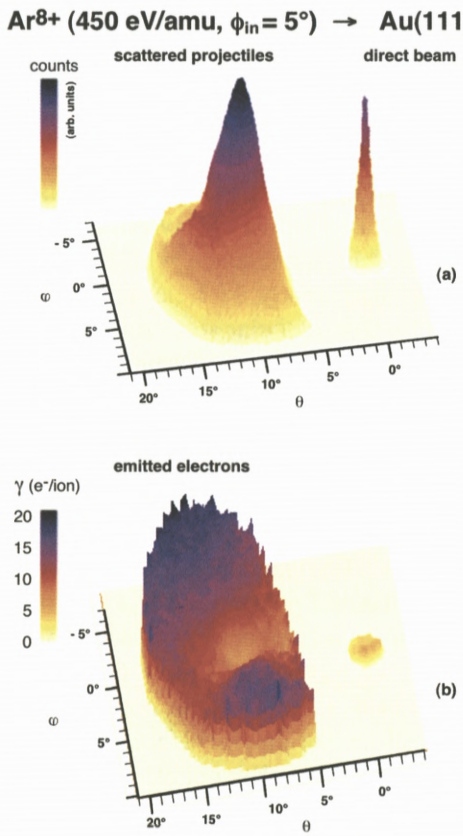

Figure 6. Top: Intensity distribution of scattered projectiles recorded with a position sensitive detector for 0.45 keV/amu Ar^{8+} ions impinging under a grazing angle $\phi_{in} = 5°$ onto a clean Au(111) surface (Lemell et al., 1998). *Bottom*: Mean number of emitted electrons measured in coincidence with projectiles scattered into different exit angles (positions corresponding to the top of figure).

charged ones. Kinetic energy distributions of both neutral and charged particles can be determined by means of time-of-flight (TOF) techniques which require a well-defined time structure (short pulsing) of the projectile beam.

2.2. MCI Impact at Grazing Incidence on Au(111)

Coincidence measurements beween ES and scattered projectiles have been performed for grazing impact of slow MCI on clean monocrystalline Au(111) with an experimental setup sketched in Figure 5 (Lemell et al., 1999; Stöckl et al., 2004). Figure 6 shows the intensity distribution of scattered projectiles recorded with a

position sensitive detector for 0.45 keV/amu Ar^{8+} ion impact under an angle of incidence of 5° onto a Au(111) surface (Lemell et al., 1998). The peaked feature on the top right hand side represents a small fraction of the primary ion beam that has passed above the target (see Figure 5), whereas the broad peak results from scattered projectiles. Specularly reflected projectiles contribute to the central peak, while scattering from surface imperfections (e.g. steps) is responsible for the tail of the scattered particles distribution. On the bottom of Figure 6 one sees the mean number of electrons emitted in coincidence with different parts of the angular distribution shown on top. Apparently, less electrons are emitted for specularly reflected projectiles than for non-specular scattering.

In Figure 7 we show the ES from these measurements. The upper panel depicts "non-coincident ES" resulting from all impinging projectiles without selection. "Coincident ES" are obtained in coincidence with projectiles for the complete scattering distribution shown in the top part of Figure 6. From the difference we see that a considerable fraction of the projectiles has not been specularly scattered and apparently produced a comparably higher electron yield.

In the center of Figure 7 ES labelled (1) results from truly specularly reflected projectiles into the central peak in the top part of Figure 6. ES labelled (2) was measured coincidently for projectiles scattered out of the specular direction into the tail shown in the top part of Figure 6. ES(2) clearly gives a higher electron yield than ES(1) [40]. Finally, in the bottom part of Figure 7 an ES is shown for Ar^{8+} impact under normal incidence on polycrystalline Au with a total impact energy of 2.5 eV/amu (Kurz et al., 1992), which is comparable to the 3.4 eV/amu kinetic energy component normal to the surface for grazing incidence of 450 eV/amu projectiles at 5o with respect to the surface. Since 100 eV (2.5 eV/amu) Ar projectiles ($v = 2.2 \times 10^4$ m/s) can hardly produce any KE, the ES shown in the bottom part of Figure 7 results exclusively from PE by Ar^{8+} ions which release a total potential energy of about 600 eV upon their surface impact. The similarity of this ES and the one labeled (1) in the center of Figure 7 proves that specular scattering from a metal surface produces approximately the same PE yield as the same ions if impinging perpendicular with an energy comparable to the surface-normal impact energy component for grazing incidence. ES(1) can therefore be related to PE from projectiles which approach the top-most surface layer not closer than about 1 a.u. Another conclusion from this observation is that the PE contribution from hollow-atom relaxation above a metal surface only depends on the respective perpendicular impact velocity component.

We remark that the tail toward higher eletron numbers in ES(1) (center of Figure 7) results from projectiles which have produced KE on some surface steps and were then just randomly scattered into the specular direction.

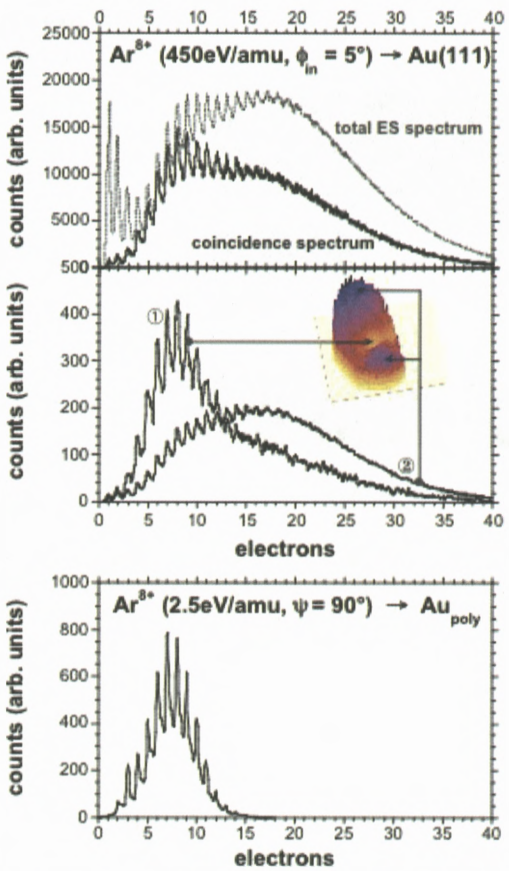

Figure 7. Top: ES for 0.45 keV/amu Ar^{8+} ions impinging under a grazing angle $\phi_{in} = 5°$ onto a Au(111) surface, measured non-coincidently and in coincidence with all scattered projectiles (Lemell et al., 1998), respectively. *Center*: ES for 0.45 keV/amu Ar^{8+} ion impact under a grazing angle $\phi_{in} = 5°$ onto a Au(111) surface, measured in coincidence with the central part (1) and the wings (2) of the projectile scattering distribution shown on top of Figure 6, respectively. *Bottom*: ES for 2.5 eV/amu normal incidence of Ar^{8+} on polycrystalline Au (Kurz et al., 1992).

In this context we note that for grazing scattering of MCI on flat surfaces the entrance angle of the MCI and therefore also the exit angle of specularly reflected neutralized projectiles are increased by the image charge attraction on the incoming trajectory (Aumayr et al., 1993a; Lemell et al., 1996b; Meyer et al., 1995; Winter, 1992). For example, near a Au surface (work function $W = 5.1$ eV) Ar^{8+} ions gain about 30 Ev, which is a considerable fraction of their initial perpendicular energy of about 140 eV in the above discussed case. For

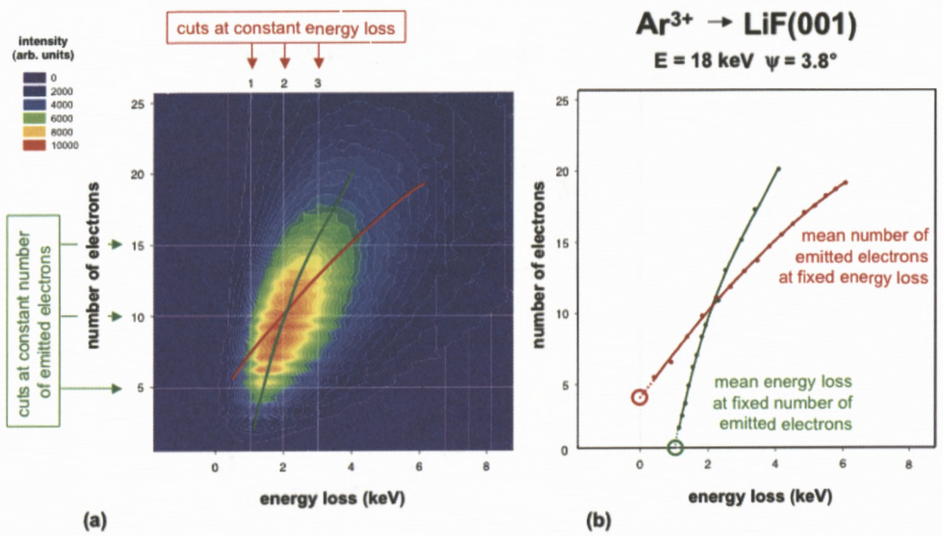

Figure 8. (a) Coincidence spectra of the number of emitted electrons *versus* projectile energy loss for 18 keV Ar^{3+} impact on a LiF(001) surface (angle of incidence 3.8°) (Stöckl et al., 2004). Red and green curves as explained in (b). (b) Cuts through these coincidence spectra at constant mean energy loss (red curve) provide the related mean number of emitted electrons, and cuts for a given mean number of emitted electrons (green curve) provide the related mean energy loss. The two curves have been extrapolated to zero energy loss and zero number of emitted electrons (red and green circle), respectively (for further explanations, see text).

higher ion charge states the increasingingly stronger image charge acceleration will eventually prohibit access to the grazing incidence regime. Secondly, faster grazing incident projectiles can produce KE by elastic collisions with quasi-free electrons above the surface (see Section 3). However, in the here discussed case the Ar ions with about 0.1 a.u. velocity give rise to a KE yield of less than 2% (Kurz et al., 1992), which is negligible in comparison to the resulting PE yield.

2.3. MCI Impact at Grazing Incidence on LiF(001)

We now consider a case where the PE and KE yields are of comparable importance. In order to separate these KE and PE contributions, we use the close relationship between KE and the inelastic energy loss of scattered projectiles (see Section 3). For grazing incidence conditions and with a time-of-flight (TOF) unit added to the setup shown in Figure 5 we have performed ES measurements in coincidence with the projectile energy loss (Stöckl et al., 2004). Figure 8 depicts a correlation of the mean number of emitted electrons with the projectile energy loss. Extrapolation of the resulting curve to the hypothetical case of projectiles

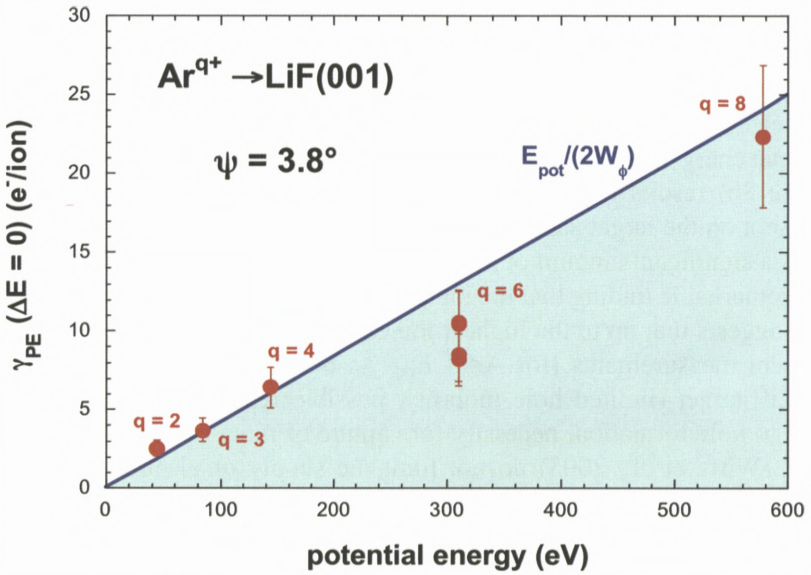

Figure 9. "Pure" PE yields *versus* MCI potential energy (data points) for grazing impact of Ar^{q+} (angle of incidence $\psi = 3.8°$) compared with theoretical limitation by potential energy conservation (solid line) (Stöckl et al., 2004).

without energy loss (red circle in Figure 8; not directly accessible in our experiment) leads to an electron emission yield which is not accompanied by a kinetic energy loss ΔE of the projectile (Stöckl et al., 2004). Therefore, this extrapolated electron yield could only result from the projectile potential energy Epot as a "pure" potential electron emission yield γ_{PE} ($\Delta E \rightarrow 0$). Plotting this extrapolated data for different Ar^{q+} projectiles as a function of the related potential energy supports our interpretation quite convincingly. As shown in Figure 9, we find a linear relationship between this "pure" PE yield and the potential energy carried by different MCI towards the surface. There is no dependence on the kinetic projectile energy which has been varied between 18 and 54 keV (Stöckl et al., 2004). Most notably, the data points are close to the limit of potential energy conservation (solid line in Figure 9). Auger processes resulting in PE (see Section 1) require a potential energy of at least twice the minimum electronic binding energy W at the surface (corresponding to the work function of metal targets). The maximum possible number of electrons emitted via PE is therefore given by $n_{max} = E_{pot}/2W$. This number of PE electrons is indeed evaluated from our extrapolated data, taking into account a binding energy of about 12 eV (Ochs et al., 1997) for the highest occupied states in the $F^-(2p)$ valance band of LiF (solid line in Figure 9).

Here we have assumed 100% probability for electron escape from the surface. This assumption seems not unreasonable considering the large band gap of LiF(001) which extends above the vacuum energy and thus blocks the absorption of slow electrons inside the solid. We also remark that the extrapolated relatively large mean energy loss of 1 keV correlated with no electron emission (green circle in Figure 8b) results from the relatively small distance of 13 cm between the impact spot on the target surface and the projectile detector, which therefore also registers a significant amount of scattering events from deeper surface layers.

Our remarkable finding that the ion potential energy is utilized by almost 100% for PE suggests that up to the highest ion charge state/potential energy applied in the present measurements (for Ar^{8+} $E_{pot} \approx 600$ eV), the electronic properties of the LiF target (limited hole mobility, possible reduction of electron capture rate due to hole formation, necessity for capture of more tightly bound electrons, see, e.g., Wirtz et al., 2003) do not limit the supply of electrons for complete neutralization and de-excitation within the given short surface interaction time.

In particular, the PE yields observed for grazing Ar^{q+} impact are by more than a factor of two larger than earlier measured for normal incidence of Ar^{q+} on polycrystalline LiF (Vana et al., 1995b). In grazing collisions the projectiles interact with many different F^- sites over a relatively long way. On the other hand, for normal impact the rates for electron capture from neighboring sites are considerably (typically one order of magnitude) smaller than for capture from the F^- ion closest to the projectile impact site, and multiple capture from a single site would also involve more tightly bound electrons (Wirtz et al., 2003). Our present findings are consistent with image charge acceleration measurements for grazing scattering of MCI on a monocrystalline LiF surface (Auth et al., 1995), from which result a complete projectile neutralization along the particle trajectory can be concluded.

Since surface-channeled projectiles interact with the surface along well defined and calculable trajectories (Winter, 2002), the here presented technique allows, at least in principle, investigations of the PE yield as a function of the closest distance of projectile approach toward the surface, which also permits studies of distance dependent Auger transition rates (Hecht et al., 1997; Monreal et al., 2003; Bandurin et al., 2004).

3. Near-Threshold Studies for KE from Grazing Incidence of Slow Atoms on Single-Crystalline Metal and Insulator Surfaces

For these measurements fast neutral atoms have been produced by passing the respective singly charged ions through a gas-filled charge-exchange cell and suf-

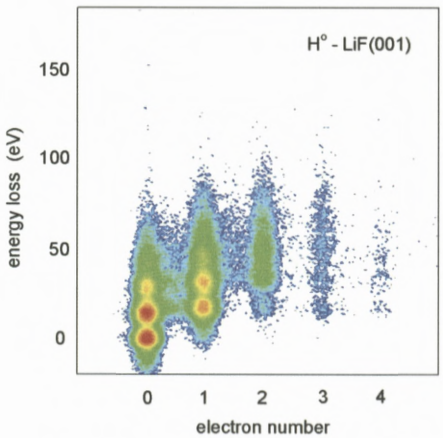

Figure 10. Raw data for projectile time-of-flight *versus* electron number for 1 keV H^0 impact on LiF(001) at $\phi_{in} = 1.8°$ (colour code indicates from blue to red increasing relative intensities; Winter et al., 2002).

ficiently close collimation. With similar techniques as described in Section 2.3, coincident measurements of electron number statistics (ES) with projectile time-of-flight have been performed for grazing scattering of neutral ground state hydrogen atoms (avoiding any PE) on LiF(001) (Winter et al., 2002), and of neutral ground state hydrogen and noble gas atoms on Al(111) (Lederer et al., 2003). This permitted precise measurements down to very small electron yields ($\leq 10^{-4}$ electrons per projectile) and also projectile energy loss measurements without electron emission, as necessary near the KE threshold.

3.1. Near-Threshold KE Studies for a LiF(001) Surface

Figure 10 shows a 2D plot of raw data for ES *versus* projectile time-of-flight (TOF) for grazing impact of 1 keV H^0 on LiF(001) (Winter et al., 2002). Events without electron emission (left column) belong to elastically scattered projectiles (lowest mark) or to a different number of discrete energy losses of 12 eV each, which are related to excitation of the corresponding number of surface excitons (Roncin et al., 1999). One- and more electron emission events (other columns) can be accompanied by production of no or of different numbers of excitons.

Figure 11 shows the electron yield and fractions of excitons and negative ions after H^0 scattering under $\phi_{in} = 1.8°$ with different impact energies. Scattered negative ions have been registered with biased electric field plates and a second particle detector (Mertens et al., 2002).

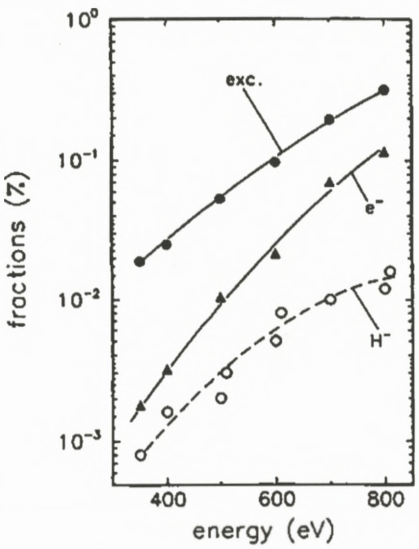

Figure 11. Fraction of excitons (full circles), electrons (full triangles) and H^- ions (open circles) *versus* impact energy, for scattering of H^0 atoms under $\phi_{in} = 1.8°$ from LiF(001) (Mertens et al., 2002).

Interpretation of these results involves the binary collision of H^0 atoms with F^- ions at LiF crystal lattice sites (Winter et al., 2002; Roncin et al., 1999; Mertens et al., 2002). In such collisions an electron can be captured from an F^- ion into a negative hydrogen state which then is shifted to a crossing with a F^{-*} surface exciton state at about 2 eV below the vacuum level. At this crossing the electron may either be recaptured for forming a surface exciton, or the negative ion prevails and acts as precursor for electron emission by detachment at the surface, or it can survive the scattering event. For grazing scattering on LiF(001) the projectile energy loss is exclusively caused by discrete contributions for exciton production (about 12 eV each) and/or negative ion formation which primarily ends up in electron detachment (about 14 eV). Toward higher impact energy the discrete energy losses gradually change into quasi-continua which however still constitute a relatively small part of the total projectile energy.

3.2. Near-Threshold KE Studies for an Al(111) Surface

The situation is rather different for a quasi-free electron metal surface such as Al(111). Figure 12 shows measured projectile energy loss distributions for emission of no and of one electron (Lederer et al., 2003). In striking contrast to

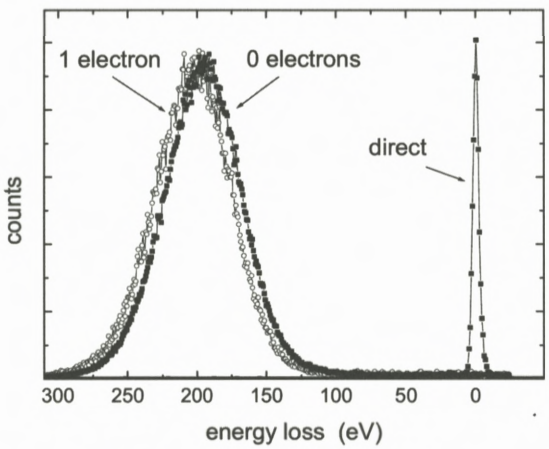

Figure 12. Energy loss spectra for emission of no (full circles) and one (open circles) electron from scattering of 1.5 keV H^0 atoms at $\phi_{in} = 1.88°$ on an Al(111) surface (Lederer et al., 2003).

scattering from LiF(001), for the metal surface the projectile mean energy loss is considerably larger but not strongly different for cases without or with emission of electrons. Apparently, most of the projectile energy loss results from friction in the quasi-free electron gas in the solid, a situation not applicable for an insulator.

The fact that without electron emission a much larger mean projectile energy loss is found for scattering from Al(111) than from LiF(001) (see Figure 10) can be satisfactorily explained with a simple classical model for binary elastic collisions of the projectile in the quasi-free electron gas at the selvedge above the Al(111) surface (Winter and Winter, 2003). The maximum velocity of electrons here is the Fermi velocity v_F which depends on the electron density. The majority of collisions takes place at a relatively large distance from the surface (typically some a.u.) and therefore results only in small projectile energy transfers which, however, for an appreciably large number of collisions along the projectile trajectory add up to the here observed total energy loss. The KE threshold velocity

$$v_{th} = \frac{v_F}{2}\left(\sqrt{1 + W/E_F} - 1\right)$$

for electron emission is reached if the energy transfer in a binary collision is sufficiently large to excite an electron from the Fermi level (EF: Fermi energy) into vacuum (Baragiola et al., 1979). Measurements performed with H^0 and He^0 projectiles agree on a quantitative level with these simple model calculations, both with respect to the KE threshold velocity vth and the dependence of the KE yield on the projectile velocity near vth (see Figure 13).

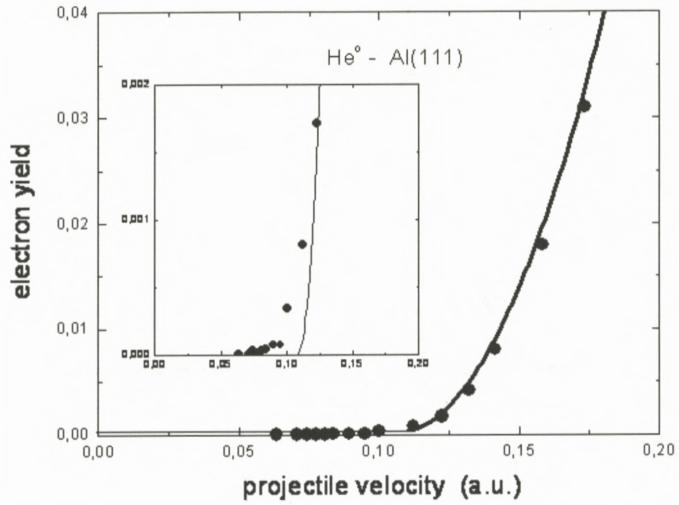

Figure 13. Full circles: Total electron yields *versus* projectile energy for He^0 atoms scattered from Al(111) under $\phi_{in} = 1.88°$. Solid curve: Model calculations as explained in the text (Lederer et al., 2003; Winter and Winter, 2003). Insert: Vertical scale enlarged by a factor of 20, with the small contribution below $v = 0.1$ a.u. presumably caused by scattering events on surface imperfections.

Recently, similar measurements have been conducted for grazing incidence of Ne and Ar atoms on Al(111). They revealed defined but very small KE contributions below the here discussed KE threshold for quasi-free electron metals. Such "subthreshold KE" has recently been explained by higher-momentum components in the local S-DOS as the result from surface corrugation and electron correlation effects (Winter et al., 2005).

Comparing Figure 11 for impact of H^0 on LiF(001) with Figure 13 for He^0 on Al(111) shows a clearly different behaviour of KE yields towards low impact energy. There is a quite well defined threshold for Al(111), whereas for LiF(001) no such clear threshold can be found even at lower impact energy than covered by Figure 11.

For insulators KE can still occur at very low impact energy, despite the generally higher electron binding energy in comparison with metal surfaces. This explains why bombardment of oxidized ("dirty") metal surfaces with slow projectiles gives a higher chance to emit electrons than for atomically clean metal surfaces. However, for non-grazing impact the observed relatively higher electron yields for insulators then for metals are mainly caused by a larger mean free

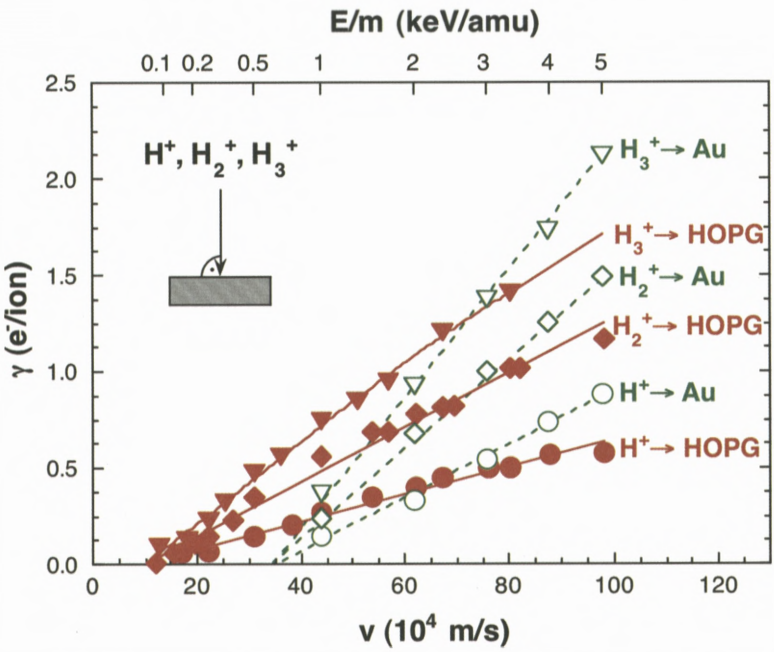

Figure 14. Comparison between total electron yields *versus* impact velocity for normal impact of H^+, H_2^+ and H_3^+ on Au and highly oriented pyrolytic graphite (HOPG) (from Cernusca et al., 2002).

path for inelastic electron collisions (KE step 2) (Hasselkamp, 1992; Schou, 1988; Rösler and Brauer, 1991).

4. Non-Proportionality Effects for Slow Molecular-Ion Induced KE

In the present context we understand as "non-proportionality" or "non-additivity" in KE a discrepancy between the KE yield for a certain molecular projectile and for the sum of KE yields produced by its constituent particles with equal impact velocity. Such effects are generally explained by differences in the projectile ion charge shielding inside the target bulk. The most simple case is KE for H_2^+ and H_3^+ molecular ions in comparison with protons. Figure 14 shows related data for normal impact of H_n^+ ($n = 1, 2, 3$) on gold (Lakits et al., 1989b) and HOPG (highly oriented graphite) (Cernusca et al., 2002). In both cases the measured electron yields are not subject to any PE contribution. Respective KE thresholds are the same for all three projectile ion species, but the KE yields themselves exhibit a clearly apparent non-proportionality. This behaviour has been explained

(Lakits et al., 1989b) by the different number of electron(s) per proton for the three projectile ions, which causes accordingly different shielding of proton(s) inside the solid. In essence, the following simple relation holds at a given impact velocity:

$$\gamma(H_n^+) = \gamma(H^+) + (n-1)\gamma(H^0).$$

This relation permits determination of KE yields for impact of neutral hydrogen atoms (which have actually been measured for a gold surface by means of the ES method; see Lakits et al., 1989b) from the much easier measurable KE yields for charged projectiles. We do not claim, however, that the same relation holds for other chemical species, which would be worthwhile to check.

A rather strong non-proportionality into the other direction has been identified for impact of singly and multiply charged fullerene ions (C_{60}^{q+}) on clean polycrystalline gold. Multicharged C_{60}^{q+} ions do not produce any PE, even if their potential energy becomes sufficiently large (about 22 eV for $q = 4$), since this potential energy is apparently used for enhanced fragmentation upon surface impact (Winter et al., 1997). The KE yield for impact of ground state C^+ ions on Au (no PE) at an impact velocity of 1.2×10^5 m/s is about 0.03 electrons/ion (Eder et al., 1999). At the same impact velocity, a single C_{60}^{q+} ion produces an average of about 9 electrons, corresponding to 0.15 electrons per carbon atom! Measurements for differently charged fullerene fragments down to $n = 15$ showed practically no deviation from the KE yield proportionality with the intact fullerene molecule. It would be of interest to investigate the behaviour of KE yields toward still lower numbers of carbon constituents, in order to explain the reason for this quite huge non-proportionality effect.

5. Novel Applications of KE and PE

5.1. Surface Triangulation by Means of KE from Grazing Incident Atoms

Measurements involving grazing incident projectiles on monocrystalline target surfaces as described in Sections 2 and 3 have been conducted for planar channeling conditions. In this scattering regime the projectile trajectories can be derived from an approximated continuum potential with planar symmetry. This results in specular reflection of projectiles in front of the topmost surface layer, with an energy loss and electron emission as explained above. The scattering conditions are drastically changed if the incident beam is aligned to a low index direction of the crystal lattice. Then the projectiles will be steered along atomic strings

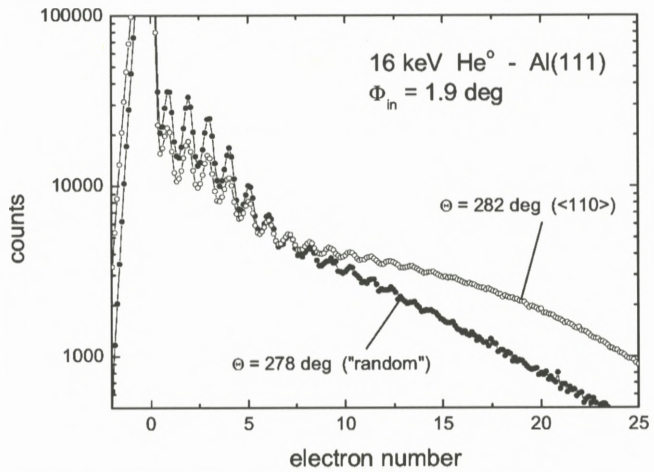

Figure 15. Non-coincident ES for scattering of 16 keV H^0 atoms from Al(111) under $\phi_{in} = 1.9°$, for azimuthal orientation angles of 282° (axial channeling) and 278° (planar scattering), respectively (Winter et al., 2004).

in the surface plane ("axial channeling"), governed by a continuum potential of axial symmetry. In such cases the probability for projectiles to penetrate into the bulk of the target becomes enhanced. Consequently, one expects for transition from planar to axial surface channeling enhanced electron yields, because of a higher chance for trajectories leading into the subsurface region. In Figure 15 we show non-coincident ES for scattering of 16 keV He atoms from Al(111) under $\phi_{in} = 1.9°$ along two different azimuthal directions (Winter et al., 2004). Data for scattering from the target surface along the ⟨110⟩ direction ($\Theta_{in} = 282°$, open circles) reveals a substantial enhancement of events with higher electron numbers, compared to a "random" azimuthal orientation ($\Theta_{in} = 278°$, full circles). This striking difference is interpreted in simple terms by a relatively small fraction of projectiles which under axial surface channeling conditions can enter the subsurface region, resulting in an increase of the total electron yield.

The such enhanced electron yield can also be observed by an increase of the (uncompensated) target current. Low index crystallographic directions can be deduced from this current as a function of the azimuthal orientation of the target surface. This "ion beam triangulation" (Pfandzelter et al., 2003) allows one to investigate the structure of clean surfaces and, in particular, ultrathin films.

Note that the data displayed in Figure 15 do not reveal a shift of ES with low electron numbers, but rather an enhancement for high electron numbers, caused by a small part of projectiles which produce a considerably larger number of

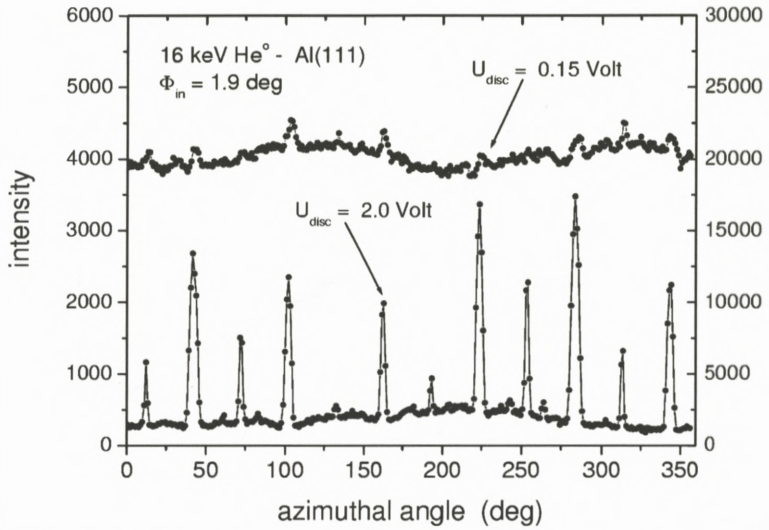

Figure 16. Electron detector count rate as function of azimuthal target angle for scattering of 16 keV He^0 atoms from Al(111) under $\phi_{in} = 1.9°$. Upper curve: discriminator level 0.15 V, lower curve: discriminator level 2.0 V (Winter et al., 2004).

electrons. With ion beam triangulation based on target current measurements, the structure of Co and Mn films epitaxially grown on Cu(001) has been studied. For these systems a variety of complex superstructures is present and, in particular, for the Mn c(12×8) Cu(001) system a new structural model has been derived (Bernhard et al., 2003). If the same method is applied by recording ES instead of the target current, important advantages will be gained. The number of impinging projectiles can be reduced to an extremely low limit of some 1,000 projectiles per second (equivalent to currents of sub-fA), so that even for ultrathin films any damage by the fast projectiles can be excluded. In addition, by selecting emission events with a higher number of electrons (see Figure 15), the "signal to noise ratio" will be substantially enhanced. This was demonstrated in the scattering experiments mentioned above by different settings of the signal discriminator level for the surface barrier detector (Winter et al., 2004). In Figure 16 resulting counts are plotted as function of the azimuthal angle for $U_{disc} = 0.15$ Volt (just above the detector noise level, upper curve) and 2.0 Volt (only detection of events with electron number $n > 9$, lower curve). Recently this new technique was successfully applied to studies on the structure of ultrathin Fe films on Cu(001) (Bernhard et al., 2005).

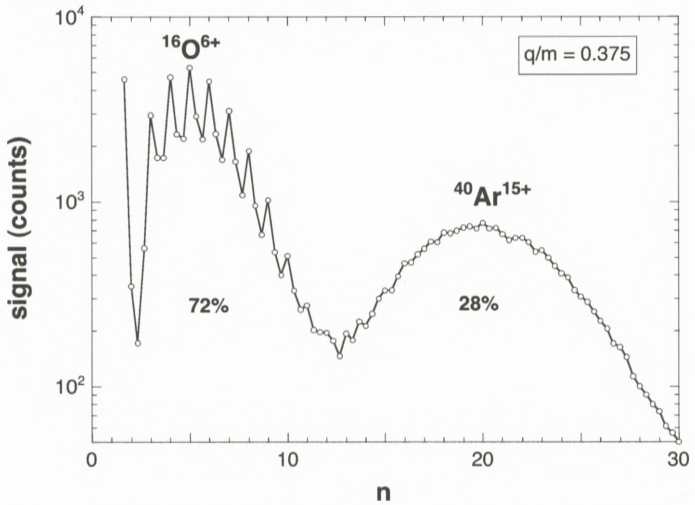

Figure 17. ES for impact of a mixed MCI beam ($^{16}O^{6+}/^{40}Ar^{15+}$) from an electron beam ion trap (EBIT) (Schneider et al., 1991). The fractions of the two ion species can be determined after evaluation of raw ES data (open circles) according to Lakits et al., 1989b and Aumayr et al., 1993b.

5.2. m/q Discrimination for Mixed Multicharged Ion Beams

Ion beams from MCI sources often comprise a mixture of ion species from different elements in different charge states. No standard methodology for ion analysis (electrostatic or magnetic field selectors, time-of-flight measurement) can distinguish between different ion species with (nearly) equal mass to charge (m/q) ratio accelerated by the same potential difference. However, one can utilize surface impact of the ions in question, as soon as they produce strongly different electron emission yields. In this way we could accurately determine the fractions of different ion species with equal q/m in mixed ion beams, both for highly charged atomic ions (different PE yields; see Figure 17 from Aumayr et al., 1993b) and for fullerene ions and their fragments (different KE yields; see Section 4 and Figure 18 from Aumayr et al., 1997).

Recently we have built a simple setup that exploits the strongly different PE yields for highly charged ions extracted from an electron beam ion trap (EBIT) of the distributed "LEIF" (low-energy ion beam facility) infrastructure in Heidelberg (Crespo López-Urrutia, 2003). An ES detector (see Section 2.1) registers short electron pulses which are created from individual ion impacts on a sputter-cleaned single-crystalline gold surface in UHV.

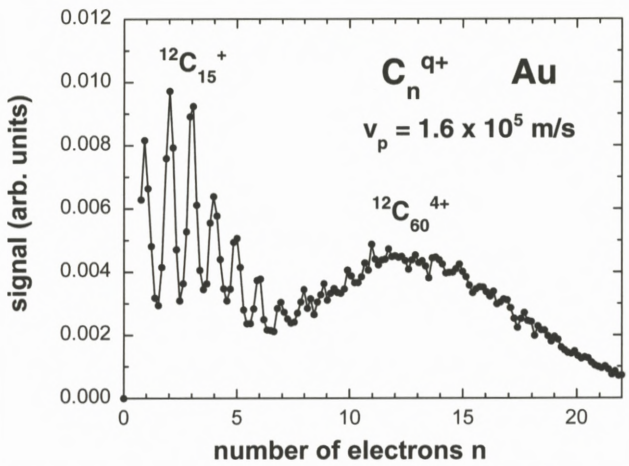

Figure 18. ES for impact of quadruply charged fullerene ions $^{12}C_{60}^{4+}$ and their singly charged fragment ions $^{12}C_{15}^{+}$ (from Aumayr et al., 1997).

The heights of these pulses are directly proportional to the number of ejected electrons. Therefore, the pulse height spectra allow for separation and quantitative analysis of different ion species with equal or nearly equal m/q. We demonstrate the power of this method by characterizing a full scan of the analyzing magnet by correlation of the pulse heights from the ES detector with the analyzing magnetic field strength. The resulting 2-D plot is shown in Figure 19 and allows one to distinguish the here desired $^{129}Xe^{q+}$ ions from various residual gas ions like Ar^{q+}, O^{q+} and N^{q+}, and to identify minute admixtures like W^{q+}, Ba^{q+} and Cu^{q+} (Meissl et al., 2006).

The target crystal was mounted on a manipulator and could easily be retracted after the here described ion identification, in order to allow the MCI beam from the electron beam ion trap to enter an experimental chamber for other measurements of interest.

6. Summary and Open Questions

R.A. Baragiola, one of the pioneers in the field of ion-induced electron emission from solid surfaces, has recently listed the following five "unsolved problems" (Baragiola, 2005):

(a) threshold behavior for heavy ions;

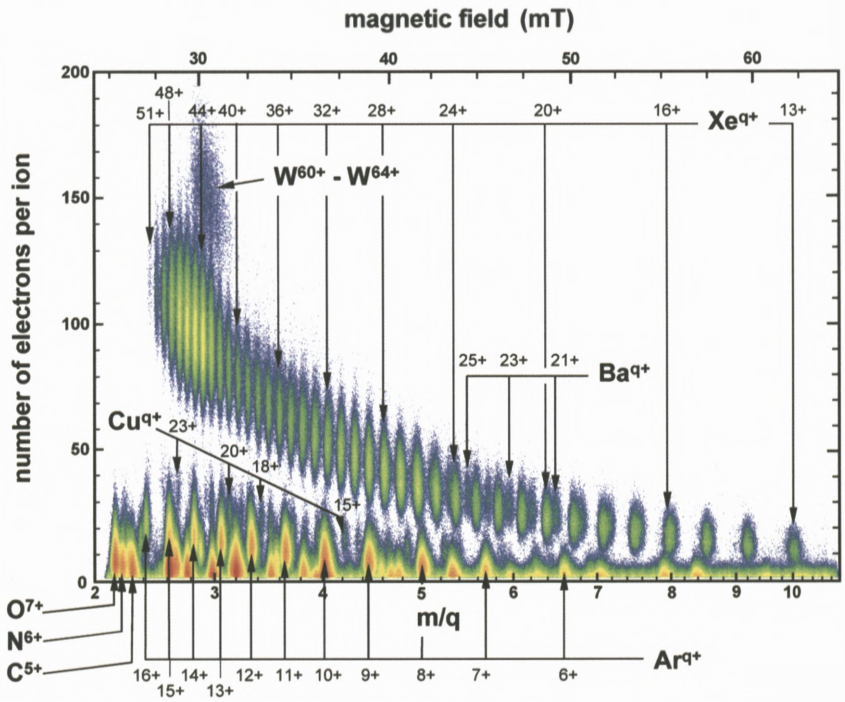

Figure 19. Plot of the number of emitted electrons for ion impact events *versus* analyzer magnet field strenght converted to ion charge-to-mass ratio (total scanning time 30 min) (Meissl et al., 2006).

(b) non-additivity in molecular impact;

(c) dependence of material properties for insulators;

(d) dynamics of plasmon decay;

(e) non-Poissonian probability for non-electron emission.

In this review we have demonstrated how the measurement of electron number statistics (ES) can benefit experimental studies on slow ion induced electron emission in a number of ways. Combination of the ES technique with grazing incidence scattering of slow atoms and singly and multiply charged ions on flat monocrystalline metal and insulator surfaces permits rather detailed studies on potential electron emission (PE) and kinetic electron emission (KE) with the following achievements.

Section 2: For impact of multiply charged ions contributions by PE and KE can be separated and quantitatively explained in terms of simple model considerations.

In contrast to metal surfaces, PE yields for insulator surfaces are considerably higher for grazing incidence than for larger angle impact, which is possibly caused by incomplete hollow-atom formation in the latter case. Systematic trajectory-dependent investigations of PE may eventually permit the mapping of Auger transition rates *versus* surface distance.

Section 3: Total electron yields for KE could be reliably measured in coincidence with the energy loss of scattered projectile down to less than 10^{-4} electrons/particle near the KE threshold. Atom trajectories with different, well defined distances of closest approach to the surface lead to KE thresholds that depend sensitively on the electron density in the surface selvedge. With these results important contributions for the solution of Baragiola's problems (a), (c) and (e) have been made.

Section 4: Examples for non-additive electron yields from molecular ion impact (problem b) suggest more systematic experiments and attention from theory. The same applies to slow ion induced plasmon excitation (problem d).

Furthermore, two interesting applications of KE and PE have been presented in *Section 5*:

(1) Based on clearly changing ES for transition from planar to axial surface channelling, a new non-destructive technique for structural characterization of surfaces and thin films ("surface triangulation") has been developed.
(2) Strongly different PE and/or KE yields permit the identification of different ion species with equal or similar q/m in mixed ion beams.

At least three other interesting points should be mentioned.

(1) The still unresolved question of a possible "trampoline effect" (Briand et al., 1996): During the approach of a slow MCI toward an insulator surface a situation could be envisaged, where still incompletely neulralized ions become stopped and reflected from the temporarily electron-depleted and thus positively charged surface.
(2) Strong electron emission from slow fullerene surface impact is not understood (Winter et al., 1997).
(3) What can be expected for grazing scattering of molecules on monocrystalline metal surfaces – will there be some kind of "snowplough" effect?

Acknowledgements

Work carried out at TU Wien has been supported by Austrian Science Foundation FWF and was carried out within Association EURATOM-ÖAW.

Work carried out at Humboldt Universität zu Berlin was supported by the Deutsche Forschungsgemeinschaft DFG (Projekt Wi 1336). HPW thanks the Alexander-von-Humboldt Foundation for generous support.

References

Arifov U.A., Kishinevskii L.M., Mukhamadiev E.S. and Parilis E.S. (1973): Auger neutralization of highly charged ions at the surface of a metal. Zh Tekh Fiz **43**, 181–187 [Sov Phys Tech Phys **18**, 118–122]

Arnau A. et al. (1997): Interaction of slow multicharged ions with solid surfaces. Surf Sci Rep **27**, 113–239

Aumayr F. and Winter HP. (2004): Potential sputtering. Phil Trans Roy Soc (London) **362**, 77–102

Aumayr F., Lakits G. and HP. Winter HP. (1991): On the measurement of statistics for particle-induced electron emission from a clean metal surface. Appl Surf Sci **47**, 139–147

Aumayr F., Kurz H., Schneider D., Briere M.A., McDonald J.W., Cunningham C.E. and Winter HP. (1993a): Emission of electrons from a clean gold surface induced by slow, very highly charged ions at the image charge acceleration limit. Phys Rev Lett **71**, 1943–1946

Aumayr F., Kurz H., Winter HP., Schneider D., Briere M.A., McDonald J.W. and Cunningham C.E. (1993b): Distinction between multicharged ion species with equal q/m. Rev Sci Instrum **64**, 3499–3502

Aumayr F., Vana M., Winter HP., Drexel H., Grill V., Senn G., Matt S., Scheier P. and Märk T.D. (1997): Distinction between multicharged fullerene ions and their fragment ions with equal charge to mass. Int J Mass Spectrom Ion Proc **163**, 9L–14L

Auth C., Hecht T., Igel T. and Winter H. (1995): Image charge acceleration of multicharged ions in front of the surface of an insulator. Phys Rev Lett **74**, 5244–5247

Bandurin Y., Esaulov V.A., Guillemot L. and Monreal R.C. (2004): Surface Miller index dependence of Auger neutralization of ions on surfaces. Phys Rev Lett **92**, 017601

Baragiola R. (1993): Electron emission from slow ion-solid interactions. In: Rabalais J.W. (Ed.), Low Energy Ion-Surface Interactions. Wiley, Chap. IV

Baragiola R.A. (2005): Some challenging unsolved problems in atomic collisions in solids. Nucl Instrum Meth Phys Res B **237**, 520–524

Baragiola R.A. and Dukes C.A. (1996): Plasmon-assisted electron emission from Al and Mg surfaces by slow ions. Phys Rev Lett **76**, 2547–2550

Baragiola R.A., Alonso E.V. and Olivia-Florio A. (1979): Electron emission from clean metal surfaces induced by low-energy light ions. Phys Rev B **19**, 121–129

Bernhard T., Pfandzelter R. and Winter H. (2003): Growth and structure of Mn and CoMn on Cu(001) studied by ion scattering. Surface Sci **543**, 36–46

Bernhard T., Baron M., Gruyters M. and Winter H. (2005): Surface structure of ultrathin Fe films on Cu(001) revisited. Phys Rev Lett **95**, 087601

Bethe H.A. and Salpeter E.E. (1957): Quantum Mechanics of One- and Two Electron Systems, Academic Press, New York

Briand J.P., de Billy L., Charles P., Essabaa S., Briand P., Geller R., Desclaux J.P., Bliman S. and Ristori C. (1990): Production of hollow atoms by the excitation of highly charged ions in interaction with a metallic surface. Phys Rev Lett **65**, 159–162

Briand J.P., Thuriez S., Giardino G., Borsoni G., Froment M., Eddrief M. and Sebenne C. (1996): Observation of hollow atoms or ions above insulator and metal surfaces. Phys Rev Lett **77**, 1452–1455

Burgdörfer J., Lerner P. and Meyer F.W. (1991): Above-surface neutralization of highly charged ions: The classical over-the-barrier model. Phys Rev A **44**, 5674–5685

Cernusca S., Diem A., Winter HP., Aumayr F., Lörincik J. and Sroubek Z. (2002): Kinetic electron emission from highly oriented pyrolytic graphite surfaces induced by singly charged ions. Nucl Instrum Meth Phys Res B **193**, 616–620

Crespo López-Urrutia J.R., Bapat B., Feuerstein B., Fischer D., Lörch H., Moshammer R. and Ullrich J. (2003): Physics with highly-charged ions in an EBIT. Hyperfine Interactions **146/147**, 109–118

Eder H., Vana M., Aumayr F. and Winter HP. (1997): Precise total electron yield measurements for impact of singly or multiply charged ions on clean solid surfaces. Rev Sci Instrum **68**, 165–169

Eder H., Aumayr F. and Winter HP. (1999): Search for projectile charge dependence of kinetic electron emission from clean polycrystalline gold. Nucl Instrum Meth B **154**, 185–193

Eder H., Aumayr F., Berlinger P., Störi H. and Winter HP. (2001): Excitation of plasmons by impact of slow ions on clean mono- and polycrystalline aluminum. Surf Sci **472**, 195–204

Gnaser H. (1999): Low-Energy Ion Irradiation of Solid Surfaces. Springer, Berlin

Hagstrum H.D. (1954a): Auger ejection of electrons from tungsten by noble gas ions. Phys Rev **96**, 325–335

Hagstrum H.D. (1954b): Theory of Auger ejection of electrons from metals by ions. Phys Rev **96**, 336–365

Hagstrum H.D. (1956): Auger ejection of electrons from molybdenum by noble gas ions. Phys Rev **104**, 672–683

Hagstrum H.D. and Becker G.E. (1973): Resonance, Auger, and autoionization processes involving $He^{+}(2s)$ and He^{++} near solid surfaces. Phys Rev B **8**, 107–121

Hasselkamp D. (1992): Kinetic electron emission from solid surfaces under ion bombardment. In: Höhler G. (Ed.), Particle Induced Electron Mission II. Springer, Heidelberg, Vol. 123, p 1

Hecht T., Winter H. and McCullough R.W. (1997): New method to analyze fast metastable atomic beams. Rev Sci Instrum **68**, 2693–2697

Kurz H., Töglhofer K., Winter HP., Aumayr F. and Mann R. (1992): Electron emission from slow hollow atoms at a clean metal surface. Phys Rev Lett **69**, 1140–1143

Kurz H., Aumayr F., Lemell C., Töglhofer K. and Winter HP. (1993): Neutralization of slow multicharged ions at a clean gold surface: Total electron yields. Phys Rev A **48**, 2182–2191

Lakits G., Aumayr F. and Winter HP. (1989a): Statistics of ion-induced electron emission from a clean metal surface. Rev Sci Instrum **60**, 3151–3159

Lakits G., Aumayr F. and Winter HP. (1989b): Electronic effects in slow heavy-particle-induced electron emission from a clean metal surface. Europhys Lett **10**, 679–685

Lederer S., Maass K., Blauth D., Winter H., Winter HP. and Aumayr F. (2003): Kinetic electron emission from the selvage of a free-electron-gas metal. Phys Rev B **67**, 121405(R)

Lemell C., Winter HP., Aumayr F., Burgdörfer J. and Reinhold C. (1995): Escape probabilities for electrons emitted during the interaction of slow highly charged ions with metal surfaces. Nucl Instrum Meth Phys Res B **102**, 33–36

Lemell C., Winter HP., Aumayr F., Burgdörfer J. and Meyer F.W. (1996a): Image acceleration of highly charged ions by metal surfaces. Phys Rev A **53**, 880–885

Lemell C., Winter HP., Aumayr F., Burgdörfer J. and Meyer F.W. (1996b): Image acceleration of highly charged ions by metal surfaces. Phys Rev A **53**, 880–885

Lemell C., Stöckl J., Burgdörfer J., Betz G., Winter HP. and Aumayr F. (1998): Multicharged ion impact on clean Au(111): Suppression of kinetic electron emission in glancing angle scattering. Phys Rev Lett **81**, 1965–1968

Lemell C., Stöckl J., Winter HP. and Aumayr F. (1999): A versatile electron detector for studies on ion-surface scattering. Rev Sci Instrum **70**, 1653–1657

Matulevich Y.T. and Zeijlmans van Emmichoven P.A. (2004): Electron emission from low-energy Xe^+ ions interacting with a MgO thin film deposited on a Mo substrate. Phys Rev B **69**, 245414

Meissl W., Simon M.C., Crespo Lopez-Urrutia J.R., Tawara H., Ullrich J., Winter HP. and Aumayr F. (2006): Novel method for unambiguous ion identification in mixed ion beams extracted from an EBIT. Rev Sci Instrum **77**, 093303

Mertens A., Winter H., Stöckl J., Winter HP. and Aumayr F. (2002): Excitation vs. electron emission near the kinetic thresholds for grazing impact of hydrogen atoms on LiF(001). Phys Rev B **65**, 132410

Meyer F.W., Folkerts L., Folkerts H.O. and Schippers S. (1995): Projectile image acceleration, neutralization and electron emission during grazing interactions of multicharged ions with Au(110). Nucl Instrum Meth Phys Res B **98**, 441–444

Monreal R.C., Guillemot L. and Esaulov V.A. (2003): On Auger neutralization of He^+ ions on a Ag(111) surface. J Phys: Condens Matter **15**, 1165–1171

Neidhart T., Pichler F., Aumayr F., Winter HP., Schmid M. and Varga P. (1995): Potential sputtering of lithium fluoride by slow multicharged ions. Phys Rev Lett **74**, 5280–5283

Ochs D., Brause M., Stracke P., Krischok S., Wiegershaus F., Maus-Friedrichs W., Kempter V., Puchin V.E. and Shluger A.L. (1997): The surface electronic structure of stoichiometric and defective LiF surfaces studied with MIES and UPS in combination with ab-initio calculations. Surf Sci **383**, 162–172

Pfandzelter R., Bernhard T. and Winter H. (2003): Ion beam triangulation of ultrathin Mn and CoMn films grown on Cu(001). Phys Rev Lett **90**, 036102

Raether H. (1988): Excitation of plasmons and interband transitions by electrons. In: Surface Plasmons on Smooth and Rough Surfaces and on Gratings. Springer Tracts in Modern Physics, Vol. 111. Springer, Berlin

Riccardi P., Ishimoto M., Barone P. and Baragiola R.A. (2004): Ion-induced electron emission from MgO exciton decay into vacuum. Surf Sci **571**, L305–310

Roncin P., Villette J., Atanas J.P. and Khemliche H. (1999): Energy loss of low energy protons on LiF(100): Surface excitation and H-mediated electron emission. Phys Rev Lett **83**, 864–867

Rösler M. and Brauer W. (1991): Theory of electron emission from nearly-free-electron metals by proton and electron bombardment. In: Höhler G. (Ed.), Particle Induced Electron Mission I. Springer, Berlin, Vol. 122

Schneider D., Clark M.W., Penetrante B., McDonald J., DeWitt D. and Bardsley J.N. (1991): Production of high-charge-state thorium and uranium ions in an electron-beam ion trap. Phys Rev A **44**, 3119–3124

Schou J. (1988): Secondary electron emission from solids by electron and proton bombardment. Scanning Microsc **2**, 607–632

Sigmund P. (1993): Fundamental processes in sputtering of atoms and molecules. Mat Fys Medd Dan Vidensk Selsk **43**, 2

Sporn M., Libiseller G., Neidhart T., Schmid M., Aumayr F., Winter HP., Varga P., Grether M. and Stolterfoht N. (1997): Potential sputtering of clean SiO_2 by slow highly charged ions. Phys Rev Lett **79**, 945–948

Stöckl J., Suta T., Ditroi F., Winter HP. and Aumayr F. (2004): Separation of potential and kinetic electron emission for grazing impact of multiply charged Ar ions on a LiF(001) surface. Phys Rev Lett **93**, 263201

Stolterfoht N., Niemann D., Hofmann V., Rösler M. and Baragiola R.A. (1998): Plasmon excitation by multiply charged Ne^{q+} ions interacting with an Al surface. Phys Rev Lett **80**, 3328–3331

Vana M., Aumayr F., Varga P. and Winter HP. (1995a): Electron emission from polycrystalline lithium fluoride induced by slow multicharged ions. Europhys Lett **29**, 55–60

Vana M., Aumayr F., Varga P. and Winter HP. (1995b): Electron emission from polycrystalline lithium fluoride bombarded by slow multicharged ions. Nucl Instrum Meth Phys Res B **100**, 284–289

Vana M., Aumayr F., Lemell C. and Winter HP. (1995c): Ion induced electron emission from solid surfaces: Information content of the electron number statistics. Int J Mass Spectr Ion Proc **149/150**, 45–57

Winter H. (1992): Image charge acceleration of multi-charged argon ions in grazing collisions with an aluminum surface. Europhys Lett **18**, 207–212

Winter H.: (2002): Collisions of atoms and ions with surfaces under grazing incidence. Phys Rep **367**, 387–582

Winter H. and Winter HP. (2003): Classical model of kinetic electron emission near threshold induced by impact of atomic projectiles on a free-electron gas metal. Europhys Lett **62**, 739–745

Winter H., Auth C., Schuch R. and Beebe E. (1993): Image acceleration of highly charged xenon ions in front of a metal surface. Phys Rev Lett **71**, 1939–1942

Winter H., Lederer S., Maass K., Mertens A., Aumayr F. and Winter HP. (2002): Statistics of electron and exciton production for grazing impact of keV hydrogen atoms on a LiF(001) surface. J Phys B: At Mol Opt Phys **35**, 3315–3325

Winter H., Maass K., Lederer S., Winter HP. and Aumayr F. (2004): Kinetic electron emission for planar versus axial surface channeling of He atoms and ions. Phys Rev B **69**, 054110

Winter H., Lederer S., Winter HP., Lemell C. and Burgdörfer J. (2005): Kinetic electron emission induced by grazing scattering of slow atoms: Local probe of the Compton profile near the Fermi edge. Phys Rev B **72**, 161402(R)

Winter HP. and Aumayr F. (2002): Slow multicharged ions hitting a solid surface: From hollow atoms to novel applications. Euro Phys News **33**, 215–218

Winter HP., Vana M., Betz G., Aumayr F., Drexel H., Scheier P. and Märk T.D. (1997): Suppression of potential electron emission for impact of slow multicharged fullerenes on clean gold. Phys Rev A **56**, 3007–3010

Wirtz L., Reinhold C.O., Lemell C. and Burgdörfer J. (2003): Liouville master equation for multielectron dynamics: Neutralization of highly charged ions near a LiF surface. Phys Rev A **67**, 12903